RESEARCH ARTICLE

Immune Checkpoint Blockade Enhances Shared Neoantigen-Induced T-cell Immunity Directed against Mutated Calreticulin in Myeloproliferative Neoplasms

Cansu Cimen Bozkus, Vladimir Roudko, John P. Finnigan, John Mascarenhas, Ronald Hoffman, Camelia Iancu-Rubin, and Nina Bhardwaj

ABSTRACT Somatic frameshift mutations in the calreticulin (*CALR*) gene are key drivers of cellular transformation in myeloproliferative neoplasms (MPN). All patients carrying these mutations (*CALR*$^+$ MPN) share an identical sequence in the C-terminus of the mutated CALR protein (mut-CALR), with the potential for utility as a shared neoantigen. Here, we demonstrate that although a subset of patients with *CALR*$^+$ MPN develop specific T-cell responses against the mut-CALR C-terminus, PD-1 or CTLA4 expression abrogates the full complement of responses. Significantly, blockade of PD-1 and CLTA4 *ex vivo* by mAbs and of PD-1 *in vivo* by pembrolizumab administration restores mut-CALR–specific T-cell immunity in some patients with *CALR*$^+$ MPN. Moreover, mut-CALR elicits antigen-specific responses from both CD4$^+$ and CD8$^+$ T cells, confirming its broad applicability as an immunogen. Collectively, these results establish mut-CALR as a shared, MPN-specific neoantigen and inform the design of novel immunotherapies targeting mut-CALR.

SIGNIFICANCE: Current treatment modalities for MPN are not effective in eliminating malignant cells. Here, we show that mutations in the *CALR* gene, which drive transformation in MPN, elicit T-cell responses that can be further enhanced by checkpoint blockade, suggesting immunotherapies could be employed to eliminate *CALR*$^+$ malignant cells in MPN.

INTRODUCTION

Immune-based therapies have revolutionized the treatment of cancer, resulting in unprecedented response rates and even complete remission (1, 2). Inhibition of immune checkpoint receptors, such as PD-1 and CTLA4, in particular, have proved successful in the treatment of several different tumor types, and their combination with other modalities is also gaining approval. Blockade of PD-1 and CTLA4 signaling, either alone or in combination, has been reported to reinvigorate tumor antigen-specific T cells, thereby ameliorating antitumor activity (3, 4). The clinical efficacy of these immunotherapies is correlated in part with mutation load and is likely based on restoring T-cell recognition of neoantigens, non-self antigens that arise from somatic

Tisch Cancer Institute, Icahn School of Medicine at Mount Sinai, New York, New York.

Note: Supplementary data for this article are available at Cancer Discovery Online (http://cancerdiscovery.aacrjournals.org/).

C. Iancu-Rubin and N. Bhardwaj are co-senior authors of this article.

Corresponding Author: Nina Bhardwaj, Tisch Cancer Institute, Icahn School of Medicine at Mount Sinai, Hess Center for Science and Medicine, 1470 Madison Avenue, Room 116, New York, NY 10029. Phone: 212-824-8427; Fax: 646-537-9571; E-mail: nina.bhardwaj@mssm.edu

Cancer Discov 2019;9:1192–207

doi: 10.1158/2159-8290.CD-18-1356

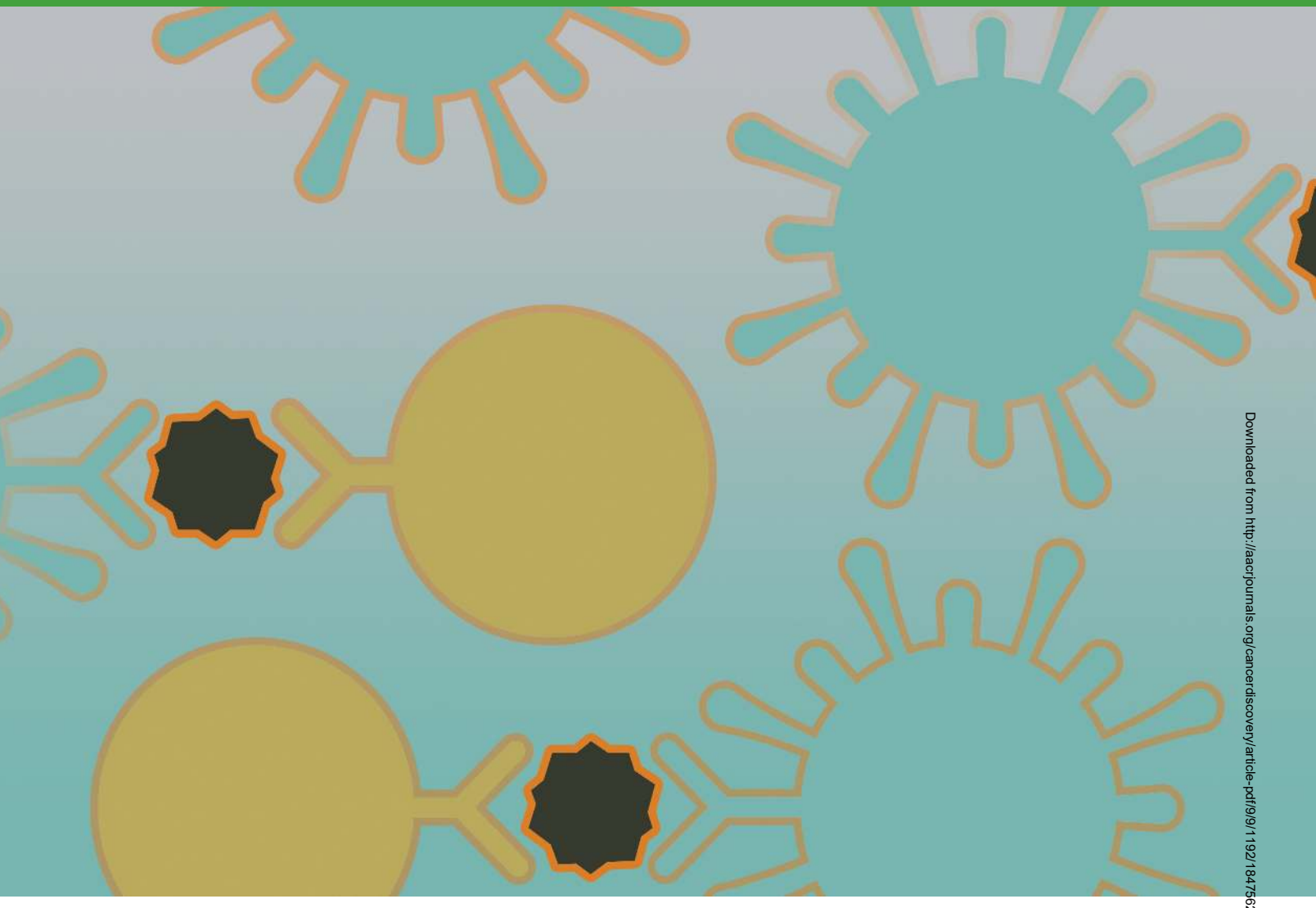

mutations in tumors, in the context of MHC molecules (3, 5–8). Neoantigen-specific T cells are not subject to immune tolerance, and hence they have the potential to exhibit strong effector responses specifically against malignant cells. However, due to intertumoral heterogeneity of mutations, neoantigen-based immunotherapies for the most part remain personalized and limited to individual patients (9, 10).

BCR–ABL1-negative myeloproliferative neoplasms (MPN), which include polycythemia vera (PV), essential thrombocythemia (ET), and primary myelofibrosis (MF), are chronic hematologic malignancies that are characterized by hyperproliferation of blood cells. The initiation and progression of MPN are associated with recurrent somatic driver mutations in Janus kinase 2 (*JAK2*), the thrombopoietin receptor gene *MPL* and calreticulin (*CALR*). Sixty-seven percent of patients with ET and 88% of patients with MF, who lack *JAK2* and *MPL* mutations, carry mutations in the exon 9 of *CALR* gene (11, 12). The mutated CALR protein (mut-CALR) mediates transformation by activating JAK–STAT signaling through its binding to MPL (13, 14). Unlike *JAK2* and *MPL* mutations, *CALR* mutations are frameshift mutations. To date, more than 50 types of insertions or deletions in the exon 9 of *CALR* gene have been reported (15). All of these mutations lead to a +1 shift in the open reading frame and result in the formation of an altered C-terminus with an identical 36-amino acid (aa) sequence that is shared by all patients with *CALR*$^+$ MPN (11). The two most frequent mutation types, L367fs*46 (type I) and K385fs*47 (type II), found in 80% of patients with *CALR*$^+$ MPN, share a 44-aa sequence (16).

Except for hematopoietic stem cell transplantation, curative treatments for patients with MPN are not available (17). Therefore, it is imperative to identify more effective treatment options for these patients. We hypothesized that the uniformity of mut-CALR marks it as an attractive MPN-specific, shared neoantigen candidate that could be targeted for the development of immunotherapy regimens for *CALR*$^+$ patients. The shared mut-CALR C-terminus is at least 36 aa long and exhibits limited similarity to wild-type (WT) CALR (16). Hence, mut-CALR could incorporate multiple epitopes, which if presented on MHC could elicit antitumor T-cell responses with minimal cross-reactivity to WT protein expressed on nonmalignant cells. We therefore evaluated

the immunogenicity of mut-CALR and found that a subset of patients with *CALR*$^+$ MPN indeed develops specific T-cell responses against mut-CALR that can be detected *in vitro*.

We also considered that an exhausted state, driven by chronic antigen exposure, might blunt the detection of mut-CALR responses in some patients. Therefore, we determined whether the expression of checkpoint molecules, namely PD-1 and CTLA4, regulated mut-CALR–specific T-cell immunity. We report here that blockade of PD-1 and CTLA4 signaling in patients with *CALR*$^+$ MPN led to both *in vivo* and *ex vivo* clonal expansion of T cells recognizing mut-CALR. Together, our results support the development of immunotherapy approaches targeting mut-CALR, either in the form of neoantigen-specific vaccines or adoptive T-cell therapies for elimination of malignant clones, and also provide a rationale for testing immune checkpoint blockade in patients with *CALR*$^+$ MPN.

RESULTS

T Cells from Patients with MPN Recognize Shared Neopeptides Originating from Somatic Frameshift Mutations in Calreticulin

Patients carrying frameshift mutations in the *CALR* gene share an identical 36-aa sequence in the C-terminus of the mut-CALR protein (11). This novel sequence exhibits limited similarity to WT CALR (16), is not expressed elsewhere, and hence is not subject to immune tolerance. Therefore, we hypothesized that the mut-CALR as a neoantigen would elicit specific T-cell responses that exhibit minimal cross-reactivity to the WT CALR. To assess whether this neoantigen could potentially elicit a cellular immune response, we investigated T-cell responses against mut-CALR neopeptide in peripheral blood mononuclear cells (PBMC) from a cohort of patients with MPN carrying *CALR* mutations. Eighteen patients with MPN with *CALR*$^+$ ET ($n = 7$), MF arising from ET (ET-MF; $n = 7$), or primary MF ($n = 4$; Supplementary Table S1) were assessed for underlying mut-CALR–specific immunity. To this end, PBMCs from patients with *CALR*$^+$ MPN were stimulated *in vitro* with pooled overlapping long peptides (OLP; 14–15 aa) spanning the mutated (Supplementary Fig. S1A) or WT (Supplementary Fig. S1B) CALR C-terminus. After expansion, the cells were restimulated with the OLP pools, and IFNγ production was measured by ELISPOT (Fig. 1A; ref. 18). A significant increase in IFNγ production was observed when the cells were stimulated with mut-CALR OLPs as compared with WT OLPs that spanned the C-terminus tail of the protein (Fig. 1B and C). Of note, mut-CALR–induced IFNγ production was observed with a greater frequency in ET, but not in patients with primary MF (Supplementary Fig. S2A–S2C). Next, we characterized the mut-CALR–specific T-cell subsets in patients with MPN by intracellular staining. Because of limitations in cell numbers, we were able to analyze 11 of the 18 patients in our cohort. Mut-CALR–induced IFNγ production, identified by comparing stimulation with mut-CALR OLPs and control peptides derived from myelin oligodendrocyte glycoprotein (MOG), was observed primarily in CD4$^+$ T cells (Fig. 1D and E). These results demonstrated that T cells from patients with *CALR*$^+$ MPN could react to mut-CALR. Yet, as T cells in these assays were stimulated with mut-CALR OLPs prior to expansion and immunogenicity evaluation, it remains possible that T cells from patients with *CALR*$^+$ MPN were primed *in vitro*. To assess directly whether *in vivo* T-cell priming has occurred in patients with *CALR*$^+$ MPN, we performed *ex vivo* T-cell ELISPOT assays using PBMCs from a total of 19 patients with *JAK2*$^{V617F+}$ MPN and 22 patients with *CALR*$^+$ MPN. PBMCs from patients with MPN were stimulated with mut-CALR OLPs or control peptides and mut-CALR–specific T-cell responses were monitored after 48 hours. No mut-CALR–specific T-cell responses were detected *ex vivo* (Supplementary Fig. S2D), suggesting either a lack of spontaneous mut-CALR–specific T-cell immunity in patients with *CALR*$^+$ MPN or limitations in the detection of responses in nonexpanded cells due to a low frequency of mut-CALR–specific T cells.

CALR protein is critical for the folding and assembly of MHC class I molecules, and CALR-deficient cells are reported to have reduced levels of cell-surface MHC class I expression as well as reduced efficiency in antigen presentation (19, 20). Therefore, we examined whether the presence of *CALR* mutations in patients with MPN was associated with a decrease in cell-surface expression of MHC molecules. Both MHC class I and II molecules were expressed by patient PBMCs (Supplementary Fig. S3A and S3B), and the expression of MHC class I molecules was significantly greater in *CALR*$^+$ MPN PBMCs than in healthy donor (HD) PBMCs (Supplementary Fig. S3A). The proinflammatory milieu that characterizes the MPNs (21), as well as certain treatment modalities, such as IFNα, among patients with MPN (22, 23) may contribute to the increased MHC class I expression. Because some of the patients in our cohort have been treated with IFNα, we assessed the role of IFNα treatment in modulating surface MHC class I expression levels. To this end, we treated cells from a *CALR*$^+$ MPN patient–derived cell line (24) with IFNα and observed a dose-dependent increase in MHC class I expression (Supplementary Fig. S3C). Importantly, CD34$^+$ cells of patients with MPN, which may harbor *CALR* mutations (25), also expressed MHC molecules (Supplementary Fig. S3D–S3F). These observations suggest that the paucity of anti–mut-CALR responses in patients with *CALR*$^+$ MPN was not due to a reduction of MHC class I expression by PBMCs or CD34$^+$ cells. Altogether, our results indicate that a subset of patients with *CALR*$^+$ MPN develop T-cell responses that are specific to mut-CALR, which are primarily of the CD4$^+$ T-cell phenotype.

Blockade of Checkpoint Receptors *In Vitro* Can Restore Mut-CALR–Specific Immune Responses

Although we observed mut-CALR–specific T-cell responses in patients with *CALR*$^+$ MPN, the responses were found only in a subset of study subjects and were of low frequency in peripheral blood. Therefore, we considered the possibility that antigen-specific T cells were undergoing exhaustion due to chronic antigen exposure. We therefore evaluated the surface expression levels of a number of immune checkpoint receptors (PD-1, CTLA4, LAG3, TIM3, TIM4, TIGIT, B7-H3, B7-H4, and VISTA) on PBMCs of patients with *CALR*$^+$ MPN. We found that MPN T cells exhibited greater degrees of expression of multiple cell-surface inhibitory molecules compared with HD T cells (Fig. 2A and B). Among these checkpoint receptors, PD-1 displayed the highest proportional

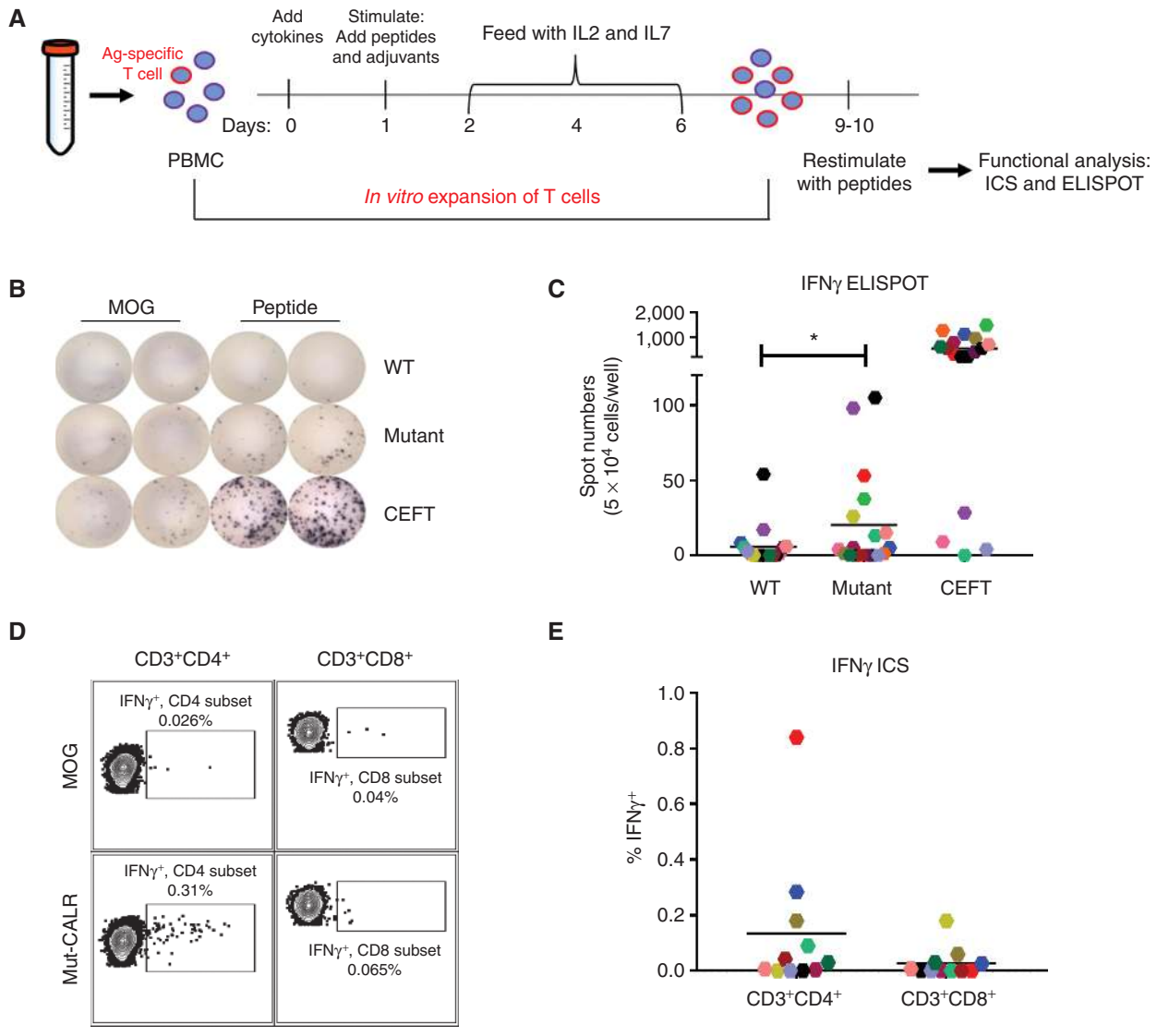

Figure 1. T-cell immunity against mut-CALR in patients with MPN. **A,** Overview of the T-cell immunogenicity assay used to evaluate antigen (Ag)-specific T-cell responses. PBMCs from patients with *CALR*$^+$ MPN were expanded *in vitro* following stimulation with WT or mut-CALR OLPs. Stimulation with a CEFT pool was used as control. Expanded T cells were restimulated with either the peptide pool they were expanded with or the control peptide pool MOG. Representative ELISPOT images (**B**) and summary of ELISPOT results (**C**) generated in PBMCs from 18 patients with *CALR*$^+$ MPN. Each data point represents one patient with MPN. Statistical significance was evaluated by Wilcoxon signed-rank test. *, $P = 0.0327$. Representative flow cytometry plots (**D**) and summary of intracellular staining analysis for IFNγ in CD4 and CD8 T-cell subsets of 11 patients with *CALR*$^+$ MPN (**E**). Statistical significance for MOG versus mut-CALR OLPs was evaluated by Wilcoxon signed-rank test. *P* values were 0.0113 and 0.3223 for CD4$^+$ and CD8$^+$ T cells, respectively. The spot numbers and % IFNγ values were calculated by subtracting the values obtained after MOG stimulation from the values after OLP pool stimulation, and negative values were set to zero. Horizontal lines indicate the mean.

increase (19.2% ± 10% in MPN vs. 3.62% ± 1.69% in HD), with expression detected in both CD8$^+$ and CD4$^+$ T-cell subsets (Fig. 2C). Similarly, increased CTLA4 expression was also detected in both T-cell subsets (Fig. 2D). On the basis of this, we hypothesized that the elevated PD-1 and CTLA4 expression could play a role in suppressing mut-CALR–specific T-cell responses. Accordingly, we reexamined mut-CALR–specific T-cell responses in *CALR*$^+$ MPN PBMCs in the context of PD-1 or CTLA4 blockade. PD-1 or CTLA4 signaling on T cells was inhibited by monoclonal blocking antibodies, and mut-CALR–specific T-cell immunity was evaluated by ELISPOT, as described in Fig. 1A–C. T-cell responses against mut-CALR OLPs were recovered in 3 *CALR*$^+$ MPNs. These cells now produced IFNγ when PD-1 or CTLA4 signaling was blocked (Fig. 2E and F). In addition to IFNγ, cells produced multiple other cytokines including TNF, suggesting that mut-CALR–specific T cells are polyfunctional (Supplementary Fig. S4). When pre- and post-checkpoint inhibition responses were combined, 11 of the 18 patients in the MPN cohort exhibited mut-CALR–specific T-cell immunity.

Apart from the increased checkpoint receptor expression, suppression of T cells in patients with cancer can be attributed

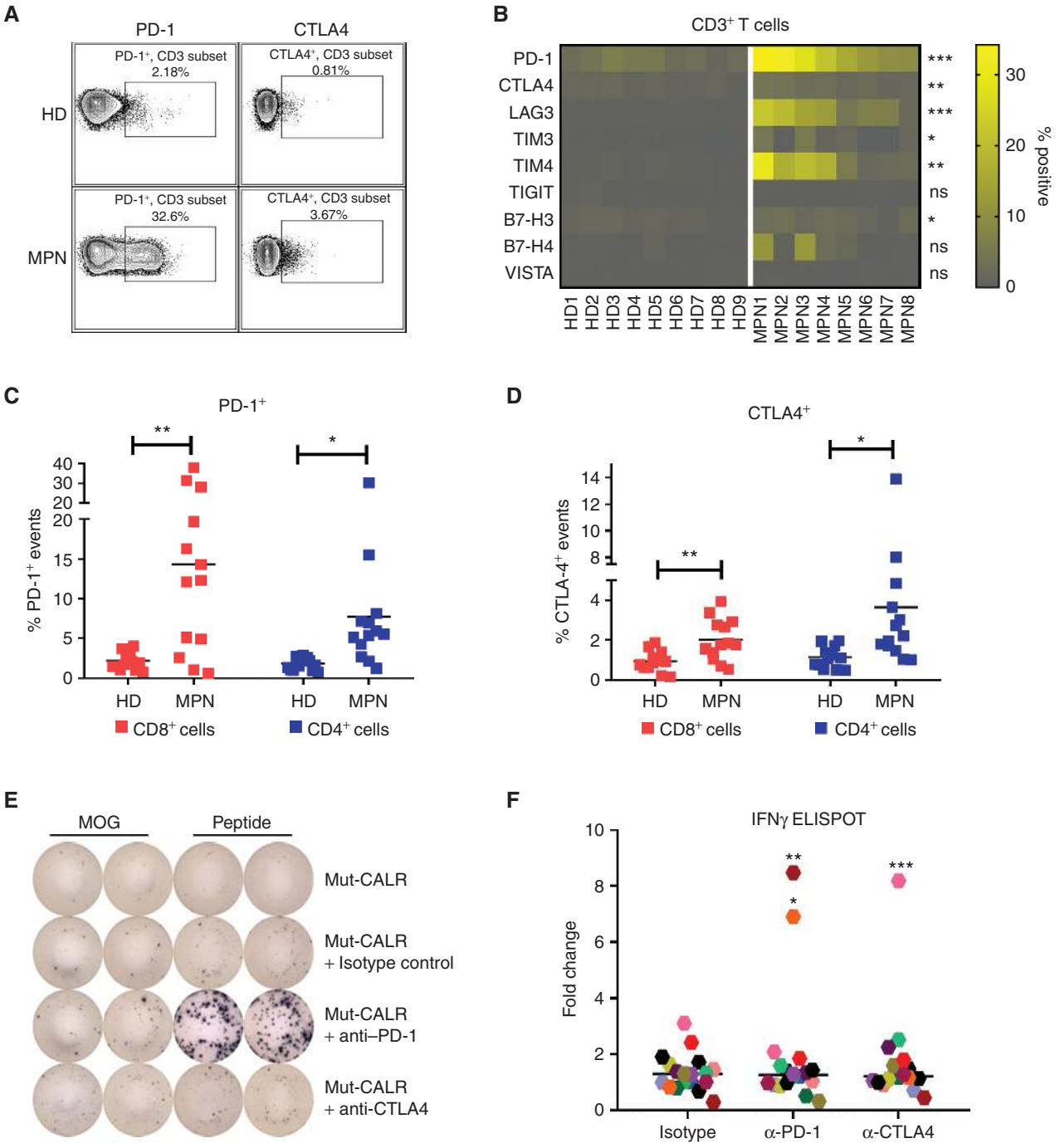

Figure 2. T cells from patients with MPN are exhausted and blockade of checkpoint receptors restores mut-CALR–specific T-cell immunity *in vitro*. **A,** Representative flow cytometric analyses showing PD-1 and CTLA4 expression in peripheral blood T cells from patients with *CALR*$^+$ MPN and HDs. **B,** Summary of flow data for cell-surface expression of checkpoint receptors, listed on the left, in HD and MPN T cells ($n = 9$ and 8, respectively). Each cell corresponds to one HD or patient with MPN. The color intensity indicates the % expression for each checkpoint receptor as gated under live, CD3$^+$ cells. Statistical significance of MPN versus HD for each checkpoint receptor was evaluated by *t* test. PD-1: ***, $P = 0.0002$; CTLA4: **, $P = 0.0037$; LAG3: ***, $P = 0.0004$; TIM3: *, $P = 0.0217$; TIM4: **, $P = 0.0051$; TIGIT: ns, $P = 0.2433$; B7-H3: *, $P = 0.0101$; B7-H4: ns, $P = 0.0615$; VISTA: ns, $P = 0.99$. Quantification of PD-1 (**C**) and CTLA4-expressing (**D**) cells within CD8$^+$ and CD4$^+$ T-cell subsets ($n = 13$ for HD and MPN). Each square represents one subject. Data were pooled from 3 independent experiments. Statistical significance was evaluated by *t* test; HD versus MPN: CD8$^+$PD-1$^+$ **, $P = 0.0014$; CD4$^+$PD-1$^+$ *, $P = 0.0106$; CD8$^+$CTLA4$^+$ **, $P = 0.0024$; CD4$^+$CTLA4$^+$ *, $P = 0.0207$. PBMCs from *CALR*$^+$ MPN patients were stimulated *in vitro* with pooled mut-CALR in the absence or presence of mAbs blocking PD-1 or CTLA-4 (10 μg/mL). Representative IFNγ ELISPOT images (**E**) and summary of ELISPOT results (**F**) generated in PBMCs from 18 patients with *CALR*$^+$ MPN. Each data point represents one patient with MPN. The change in spot numbers was displayed as fold change by dividing the number of spots formed after OLP pool stimulation to the number of spots formed after MOG stimulation. Horizontal lines indicate the median. Statistical significance for changes at population level was evaluated by Wilcoxon signed rank test. Isotype versus α-PD-1: $P = 0.3465$, isotype versus α-CTLA4: 0.4171. In addition, statistical significance was evaluated for each subject by *t* test by comparing isotype versus checkpoint blockade. Three subjects who showed significant response to checkpoint blockade were denoted. *, $P = 0.0121$; **, $P = 0.0045$; ***, $P = 0.0005$.

to the expansion of other immunoregulatory cell populations (26). Therefore, we investigated the presence of myeloid-derived suppressor cells (MDSC) and regulatory T cells (Treg) in MPN PBMCs from the same cohort. We found that MDSCs, defined as $Lin^-CD33^+CD11b^+HLA\text{-}DR^-CD14^-$ cells (27), were significantly expanded in patients with *CALR*$^+$ MPN when compared with HDs (Supplementary Fig. S5A and S5B). However, the frequencies of Treg populations, $CD4^+CD25^+FOXP3^+$, were comparable between patients with *CALR*$^+$ MPN and HDs (Supplementary Fig. S5C and S5D). We also found that the average percentage of $CD3^+$ T cells in the peripheral blood of patients with MPN was lower than in HDs (Supplementary Fig. S5E–S5G). These observations may account for why blockade of PD-1 and CTLA4 failed to rescue mut-CALR–specific T-cell responses in some patients. Together, these data indicate that peripheral blood T cells in patients with *CALR*$^+$ MPN exhibit an exhausted phenotype, and checkpoint blockade might be an effective strategy to restore mut-CALR–specific T-cell responses in a subset of patients.

PD-1 Blockade *In Vivo* Augments T-cell Responses

To gain further insights into checkpoint receptor–mediated T-cell suppression in patients with *CALR*$^+$ MPN, we took advantage of an ongoing phase I/II clinical trial (NCT03065400), in which patients with advanced MPN are undergoing treatment with pembrolizumab (Fig. 3A). One of the patients enrolled in the study expressed type I *CALR* mutation (c1092_1143del52; PT#15 in Supplementary Table S1). Using longitudinal blood samples available from this patient, we monitored the changes in the frequencies of T cells before and after pembrolizumab treatment by both flow cytometry and T-cell receptor (TCR) sequencing. Prior to therapy, only 4% of the patient's PBMCs were T cells, and of these 32% expressed PD-1 (Supplementary Fig. S6A). Importantly, the proportion of T cells in peripheral blood greatly increased after pembrolizumab treatment, reaching up to 26% and 18% of PBMCs after 2 (T1) and 6 (T2) cycles of treatment, respectively (Fig. 3B–D). Pembrolizumab treatment was accompanied by increases in both peripheral blood $CD4^+$ and $CD8^+$ T cells (Supplementary Fig. S6A). After pembrolizumab administration, PD-1–expressing T cells in peripheral blood were undetectable by commercial anti–PD-1 antibodies (Supplementary Fig. S6A), probably due to the persistent binding of pembrolizumab to PD-1 on T cells *in vivo*, as described previously (28, 29). In addition, TCR Vβ sequencing was undertaken to evaluate the extent of clonal expansion. TCR Vβ chains of peripheral blood T cells before and after pembrolizumab treatment were sequenced, and the diversity of TCR repertoire was calculated by Pielou's evenness metric. The results indicated that T cells not only expanded but also showed greater clonality after pembrolizumab treatment (Fig. 3E). After the initial treatment cycles, 8 T-cell clones were significantly expanded compared with baseline (pretreatment; Fig. 3F). Each of these clones remained significantly expanded after additional cycles of treatment and there were 15 more T-cell clones that were also significantly expanded compared with baseline (Fig. 3G). These observations suggested that *in vivo* PD-1 blockade may help reinvigorate T cells in patients with MPN.

To address this possibility, we evaluated changes in antigen-specific, namely mut-CALR–specific, T-cell responses in this patient with *CALR*$^+$ MPN prior to and during pembrolizumab administration. At baseline, peripheral blood T cells from this patient did not have detectable mut-CALR–specific responses, even after *in vitro* inhibition of PD-1 with antibody blockade. After pembrolizumab treatment, however, mut-CALR–specific T-cell responses were evident, as shown by increased IFNγ production (Fig. 3H). Interestingly, *in vitro* addition of PD-1–blocking antibody was necessary to observe such responses. We speculate that this was due to the upregulation of PD-1 expression on the T cells during the *in vitro* expansion (Supplementary Fig. S6B). Hence the blockade of PD-1 was required to uncover mut-CALR–specific responses. Next, we investigated the changes in clonal T-cell populations in these *in vitro* cultures in response to stimulation with mut-CALR OLPs. Peripheral blood T cells, collected after the initial treatment (T1), were stimulated and expanded *in vitro* with WT or mutant CALR peptides, in the absence or presence of PD-1–blocking antibodies. Subsequently, TCR Vβ chains of the expanded T cells were sequenced. Multiple T-cell clones uniquely expanded in response to stimulation with mut-CALR OLPs in the presence of PD-1–blocking antibodies (Supplementary Fig. S7A–S7D). Among these, 2 clones that also significantly expanded in peripheral blood after pembrolizumab treatment were identified (Fig. 3I). Interestingly, the frequency of 1 of these 2 clones reached above 30% in all of the *in vitro* groups. The cells utilized in these *in vitro* cultures were collected after pembrolizumab administration, and clonal expansion of T cells was evident at this point compared with baseline. We speculate that this specific clone of T cells was invigorated *in vivo* after pembrolizumab treatment and had a proliferative advantage, thereby populating the *in vitro* cultures. Although these cells might recognize mut-CALR epitopes, it remains possible that these are bystander T cells recognizing epitopes unrelated to mut-CALR (30). Together, these observations, although limited to one patient, indicate that PD-1 blockade in patients with *CALR*$^+$ MPN may lead to expansions of clonal T-cell populations that could potentially recognize neoantigens derived from mut-CALR.

Mut-CALR Reactive T Cells Can Be Elicited from Healthy Donor T Cells

Our data suggest that systemic T-cell exhaustion may limit the ability to observe mut-CALR–specific T-cell responses in patients with MPN. Schumacher and colleagues have previously demonstrated that neoantigen-specific T cells can be primed from T cells in HD blood (31). Similarly, we hypothesized that mut-CALR–specific T cells could be readily primed from HD blood. To test this hypothesis, PBMCs from 16 HDs were stimulated with OLPs derived from mut-CALR, and the responses were measured by ELISPOT and ICS. Responses to mut-CALR were observed in both $CD4^+$ and $CD8^+$ T cells and were characterized by the production of effector cytokines, such as IFNγ, as well as an increase in the surface expression of the activation marker CD137 (4-1BB; Fig. 4A–E). Importantly, the observed T-cell responses were specific to mut-CALR, as responses to stimulation with WT CALR OLPs were not higher than the background (Fig. 4A–C). Consistent with the hypothesis that T-cell exhaustion limits mut-CALR–specific T-cell responses in patients with MPN, we observed mut-CALR–specific T-cell responses in a

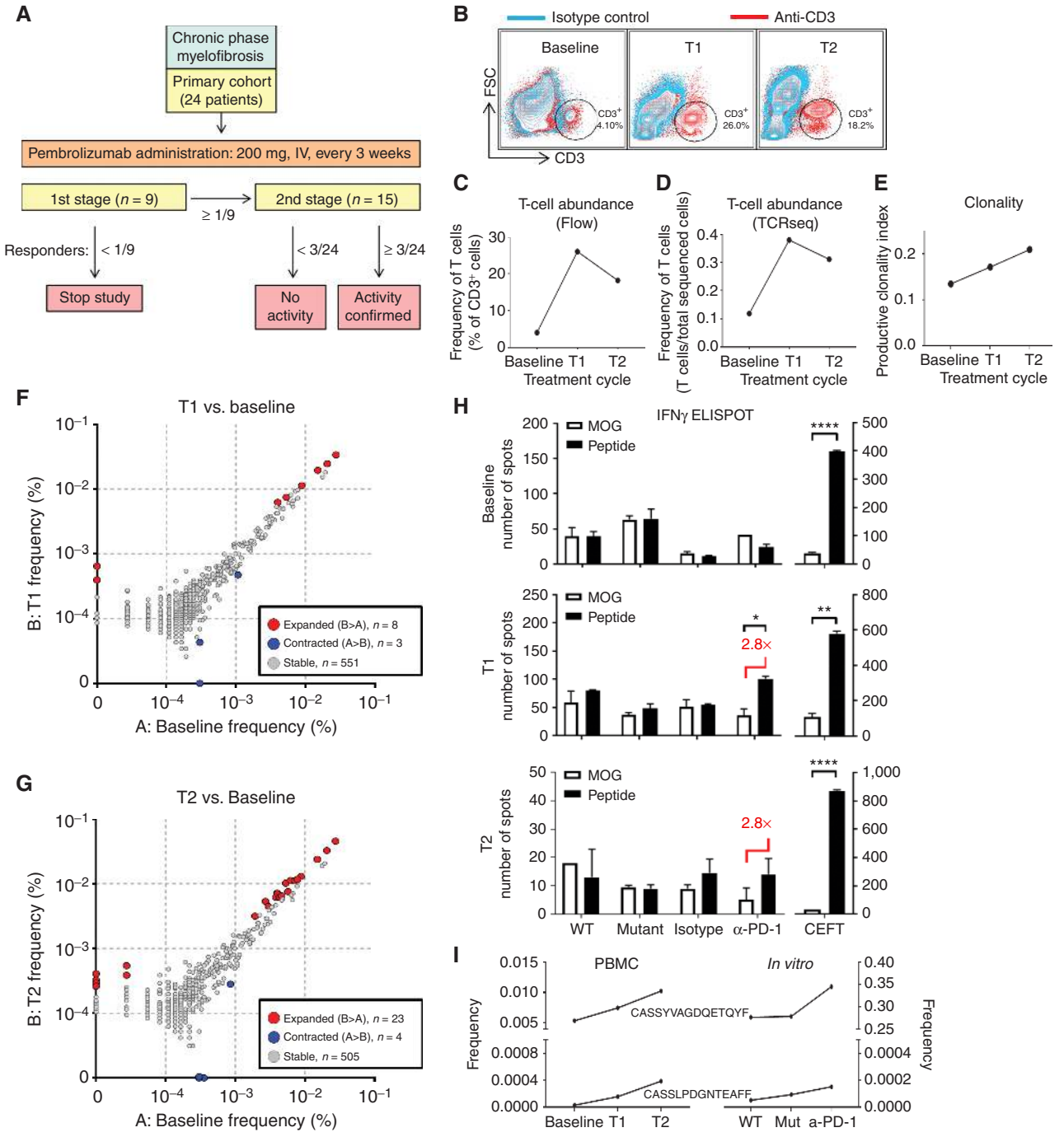

Figure 3. Pembrolizumab administration rescues mut-CALR–specific immunity. **A,** Schema of a phase I/II clinical trial to assess the efficacy, safety, and tolerability of pembrolizumab in patients with chronic phase myelofibrosis. The FDA-approved dose of 200 mg pembrolizumab is administered via intravenous infusion every 3 weeks. Nine patients will be enrolled in the first stage of the Simon two-stage design, and 15 in the second stage. A treatment cycle is 3 weeks and the core study period is 6 cycles. PBMCs were collected from a patient with *CALR*$^+$ MPN receiving pembrolizumab, before (baseline) and after 2 and 6 cycles of treatment, T1 and T2, respectively. The frequency of T cells was analyzed by flow cytometry (**B** and **C**; CD3$^+$ cells) or by TCRseq (**D**; number of cells expressing TCR/number of total nucleated cells). **E,** Clonality of T cells was calculated as 1 − Pielou's evenness. Changes in the abundance of unique TCR Vβ sequences were analyzed using the ImmunoSEQ platform: **F** and **G,** T1 versus baseline (**F**) and T2 versus baseline (**G**). Only clones with a cumulative abundance of 10 or above were included in the analysis. The binomial method was used to calculate *P* values. FDRs were controlled by the Benjamini–Hochberg method. The differential abundance of clones was considered significant (red and blue circles) when *P* value was equal to or less than 0.01. **H,** PBMCs collected at T1 were stimulated *in vitro* with either WT or mut-CALR OLPs, alone or in the presence of PD-1–blocking antibodies. IFNγ production by expanded T cells was measured by ELISPOT. Statistical significance was evaluated by *t*-test, comparing MOG and peptide stimulation for each group: a-PD-1 *, $P = 0.0168$; CEFT at baseline ****, $P < 0.0001$; at T1 **, $P = 0.0016$; at T2 ****, $P < 0.0001$. **I,** Two clones that were significantly expanded in peripheral blood upon pembrolizumab treatment were also expanded in *in vitro* cultures upon stimulation with mut-CALR OLPs when PD-1 was blocked. TCR Vβ rearrangements for each clone are indicated next to frequency graphs.

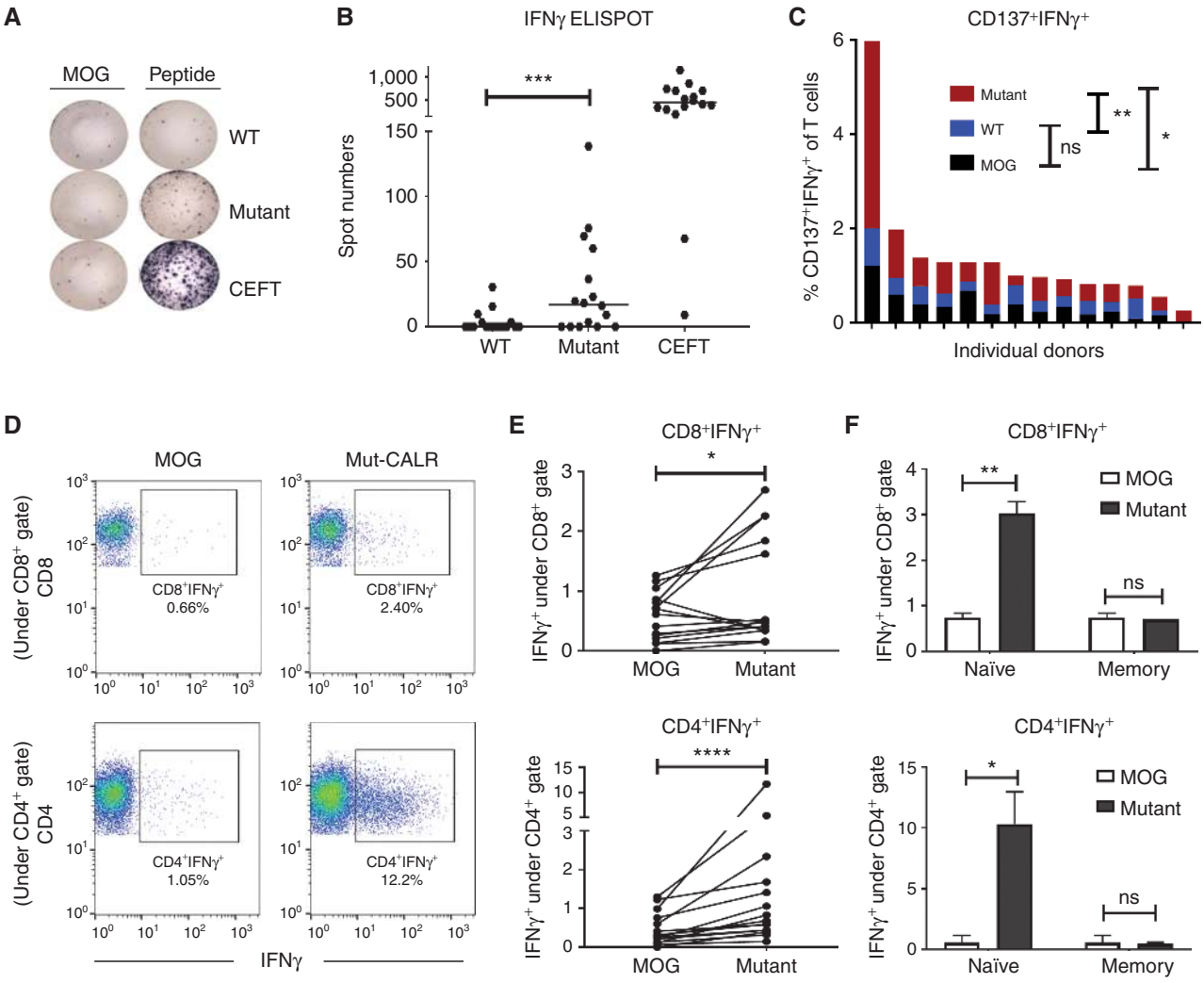

Figure 4. Healthy donors provide mut-CALR reactive T cells. PBMCs collected from healthy donors were stimulated *in vitro* with pooled WT or mut-CALR OLPs. Stimulation with a CEFT pool was used as control. Representative IFNγ ELISPOT images (**A**) and summary of ELISPOT results (**B**) generated in PBMCs from 16 healthy donors. The spot numbers were calculated by subtracting the number of spots formed after MOG stimulation from the number of spots formed after OLP pool stimulation and negative values were set to zero. *P* value was calculated by the Wilcoxon signed-rank test. ***, $P = 0.001$. Horizontal lines indicate the median. **C,** Percentage of CD137$^+$IFNγ$^+$ T cells, assessed by flow cytometry. Each bar represents an individual donor. *P* values were calculated by the Wilcoxon signed-rank test. MOG versus WT: *, $P = 0.0144$; WT versus mutant: **, $P = 0.007$. **D,** Representative flow plots showing IFNγ production by CD8$^+$ and CD4$^+$ T cells upon priming with MOG or mut-CALR OLPs. **E,** Quantitative summary of frequencies of T-cell subsets producing IFNγ ($n = 15$). *P* values were calculated by the Wilcoxon signed-rank test. *, $P = 0.0413$; ****, $P < 0.0001$. Each data point represents one healthy donor. **F,** Naïve (CD45RO$^-$CD45RA$^+$CCR7$^+$) and memory (CD45RO$^+$ CD45RA$^-$) T cells and APCs (CD3$^-$) were isolated by FACS from HD PBMCs ($n = 2$). APCs pulsed with MOG or mut-CALR OLPs were cocultured with naïve or memory T cells. IFNγ production by each T-cell population was measured by flow cytometry. *P* values were calculated by *t*-test. **, $P = 0.078$; *, $P = 0.0365$.

greater fraction of HD PBMCs than MPN PBMCs [$P = 0.001$ for HD (Fig. 4B) and $P = 0.037$ for MPN (Fig. 1C)]. In addition, T-cell responses observed in HD PBMCs were of a higher magnitude than those observed in MPN PBMCs.

Healthy blood donors presumably have had no prior exposure to mut-CALR. Therefore, any observed mut-CALR–specific T-cell response should result from effective priming of naïve mut-CALR–specific T-cell precursors. To test this hypothesis, naïve (CD3$^+$CD45RO$^-$CD45RA$^+$CCR7$^+$) and memory (CD3$^+$CD45RO$^+$) T cells and non–T-cell (CD3$^-$) antigen-presenting cells (APC) were sorted from PBMCs of reactive HD. APCs, pulsed with mut-CALR OLPs, were then separately cocultured with either naïve or memory T cells. Consistent with the hypothesis that mut-CALR–induced responses were derived from *de novo* T-cell priming, we observed mut-CALR–specific T cells in cocultures with sorted naïve T cells, but not with memory T cells (Fig. 4F). To confirm these findings, umbilical cord blood mononuclear cells, which are unlikely to have memory T cells (32), were stimulated with mut-CALR OLPs. The induction of mut-CALR–specific T-cell responses was also evident in these cultures (Supplementary Fig. S8). These data confirm the immunogenicity of the mut-CALR neoantigen and demonstrate the feasibility of priming antigen-specific T-cell responses from naïve T cells.

T Cells Recognize Multiple Epitopes in Mut-CALR C-Terminus That Are Endogenously Processed and Presented

The mut-CALR C-terminus is >36 aa long (16) and may give rise to multiple immunogenic epitopes. In addition, our tested cohorts of patients with MPN and HDs will exhibit diverse human leukocyte antigen (HLA) haplotypes. An individual's HLA alleles will determine whether they are able to present mut-CALR epitopes, which will depend upon the relative binding affinities. To this end, we interrogated the binding affinities of epitopes derived from the altered C-terminus using *in silico* peptide binding prediction algorithms through the immune epitope database (IEDB). For maximal population coverage, we used IEDB's HLA reference set that covers >97% and >99% of the population for class I and class II alleles, respectively. Our analysis showed that multiple epitopes could theoretically bind to several HLA class I and II alleles (Supplementary Fig. S9A and S9B; Supplementary Tables S2 and S3). Furthermore, HLA-I alleles with predicted high binding affinities for mut-CALR–derived epitopes (Supplementary Table S2) were represented in approximately 60% of the population of the United States, according to recorded allele frequencies of 2.9 million typed donors covering 16 races (33, 34). Hence, a significant proportion of patients with MPN with the *CALR* frameshift mutation may have the potential to develop antigen-specific T cells.

Next, we aimed to identify which, if any, of the predicted HLA-I/II-restricted epitopes could induce T-cell responses. We selected 3 HDs that displayed both $CD8^+$ and $CD4^+$ T-cell effector responses upon stimulation with the mut-CALR OLP pool. We deconvoluted the mut-CALR OLP pool by priming HD precursor T cells with individual OLPs within the pool (Supplementary Fig. S1A). We observed $CD8^+$ and $CD4^+$ T-cell responses against multiple individual OLPs (Fig. 5). We also performed sequence-based HLA-I/II genotyping (SBT) for these subjects and determined the predicted HLA-I/II binding affinities of the epitopes that induced IFNγ production by $CD8^+$ or $CD4^+$ T cells using the IEDB's recommended algorithm. Each stimulating OLP yielded epitopes that were predicted to bind strongly to the HLA alleles of the donors tested (Fig. 5), suggesting that the predicted epitope may have been responsible for the observed mut-CALR–specific T-cell response. In addition, we evaluated whether the mut-CALR epitopes predicted to be strong binders to donor HLA (percentile rank < 2) were enriched within the OLPs that induced $CD8^+$ T-cell responses. Although such enrichment was observed for each donor tested, the correlation was not significant as there were a few OLPs that did not induce T-cell responses, yet were enriched for predicted epitopes (Supplementary Fig. S9C). This observation is expected because many studies have reported that the majority of predicted epitopes fail to elicit T-cell responses (35) and that high HLA-peptide binding affinity does not equate to immunogenicity. In addition, when we perform T-cell immunogenicity assays, we start with a limited number of PBMCs, typically around 1 million. Therefore, it is possible that we may not capture all reactive T cells, especially the ones that are low in precursor frequency.

Because mut-CALR OLPs induced $CD8^+$ T-cell responses, we aimed to identify the minimal epitopes that were recognized by $CD8^+$ T cells. To perform an unbiased screening of all potential epitopes, a complete library of peptides with 9-aa length was synthesized. The 9mers overlapped with an offset of 1 aa and spanned the last 46 aa of the C-terminus of mut-CALR, formed by the 52-bp deletion. PBMCs from 3 additional HDs were stimulated with pools of these overlapping 9mers (6–7 peptides/pool) to screen for CD8 responses. CD8 responses were detected in one of the donors tested (Fig. 6A). As expected, short peptides did not induce CD4 responses (Fig. 6B). Next, we aimed to identify which epitopes within the stimulating pool (pool 1) were inducing the response. First, we investigated the predicted binding affinities of each epitope to the donor's HLA alleles. Out of the 6 epitopes constituting the pool, only "RMMRTKMRM" was predicted to have a percentile rank <2 by NetMHCpan 3.0 (Fig. 6C; Supplementary Fig. S10A). We then restimulated cells expanded with pool 1 with individual epitopes constituting the pool. In accordance with the predictions, only one epitope, "RMMRTKMRM", was recognized by $CD8^+$ T cells (Fig. 6D and E). To further confirm the immunogenicity of this epitope, we predicted the binding affinities of "RMMRTKMRM" and other related epitopes (Supplementary Fig. S10B) to common HLA class I alleles (Supplementary Fig. S10C). Next, we identified HDs with at least one HLA allele that was predicted to bind to the epitopes tested (Supplementary Fig. S10D). As an example, we observed $CD8^+$ T-cell responses in donor 5 (Fig. 6F and G), further demonstrating the immunogenicity of these epitopes. Notably, this donor carried 3 of the predicted alleles (Supplementary Fig. S10D). $CD8^+$ T cells from donor 5 produced effector cytokines both when stimulated with minimal epitopes and with a long peptide containing these epitopes (Fig. 6G). These data suggest that the identified epitopes can be processed and loaded onto MHC molecules within the cells. To further test this hypothesis, we expanded T cells from donor 5 by stimulating with the minimal epitope p10.4, and cocultured the expanded T cells with autologous APCs that were pulsed with a long peptide containing p10.4 sequence. We observed that long peptide–loaded APCs could induce p10.4-specific $CD8^+$ T cells (Fig. 6H), suggesting this epitope is endogenously processed and presented to T cells by APCs.

Together, these data show that mut-CALR can induce T-cell responses, even in HDs without prior exposure to mut-CALR. Moreover, it provides evidence that healthy donor T cells can be utilized as an alternative approach to evaluate the breadth and specificity of mut-CALR–specific T-cell responses and their HLA restriction.

DISCUSSION

In this study, we demonstrate that mut-CALR is a shared MPN-specific neoantigen that can induce T-cell responses. Our results reveal that mut-CALR elicits specific T-cell responses in patients with $CALR^+$ MPN, delineate the immunogenic properties of mut-CALR and identify a role for immune checkpoint blockade in enhancing mut-CALR–specific T-cell immunity in patients with $CALR^+$ MPN.

Recent studies from Holmstörm and colleagues and Tubb and colleagues also evaluated mut-CALR–specific T-cell immunity (36–38). Holmstörm and colleagues reported that

Donor 1, HLA typing		
	Class I	
A*	02:01:01	32:01:01
B*	39:10:01	58:01:01
C*	07:01:01	12:03:01
	Class II	
DRB1*	11:01:02	13:02:01
DRB3*	02:02:01	03:01:01
DQB1*	06:02:01	06:09:01
DPB1*	02:01:01	17:01

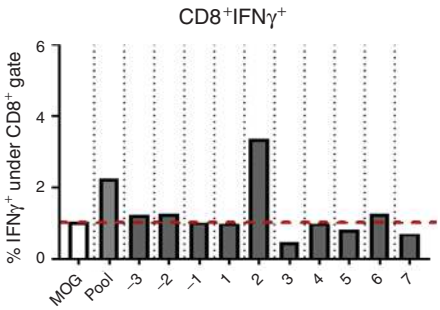

OLP	Allele	Epitope	Rank	ann_IC50	smm_IC50
2	HLA-C*07:01	MRRTRRKMR	0.39	239.87	15.71
2	HLA-C*07:01	TRRKMRRKM	0.68	165.52	25.83
2	HLA-C*07:01	RRTRRKMRR	1.67	2148.72	53.11
2	HLA-C*12:03	RRKMRRKMS	16.1	30918.15	8.55
2	HLA-C*12:03	RKMRRKMSP	22	21953.34	22.92

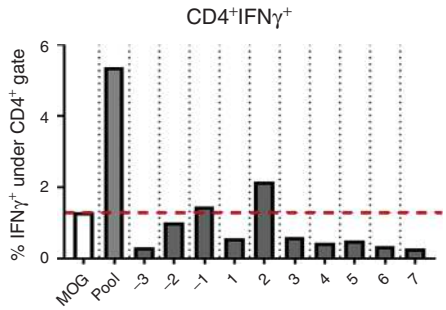

OLP	Allele	Rank	nn_align_IC50	smm_align_IC50
2	HLA-DRB1*11:01	1.91	12.5	21

Donor 2, HLA typing		
	Class I	
A*	02:05:01	26:01:01
B*	38:01:01	58:01:01
C*	07:01:01	12:03:01
	Class II	
DRB1*	04:02:01	13:02:01
DRB3*	03:01:01	
DRB4*	01:01:01	
DQA1*	01:02:01	03:01:01
DQB1*	03:02:01	06:09:01
DPA1*	01:03:01	01:03:01
DPB1*	03:01:01	04:01:01

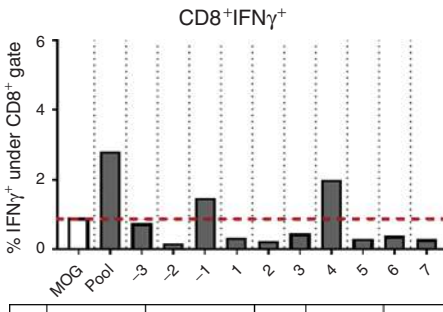

OLP	Allele	Epitope	Rank	ann_IC50	smm_IC50
–1	HLA-C*07:01	MRMRRMRRT	0.16	80.8	5.84
–1	HLA-C*07:01	MRRMRRTRR	0.43	573.47	13.78
–1	HLA-C*07:01	RRMRRTRRK	0.45	299.65	16.64
–1	HLA-C*12:03	MRMRRMRRT	32.85	16573.59	36.75
–1	HLA-C*12:03	TKMRMRRMR	34	34124.66	26.68
4	HLA-C*07:01	MSPARPRTS	1.85	7625.37	27.24
4	HLA-C*07:01	ARPRTSCRE	3.3	9467.19	77.83
4	HLA-C*12:03	PARPRTSCR	9	5521.69	13.56
4	HLA-C*12:03	MSPARPRTS	13.15	8439.26	17.96

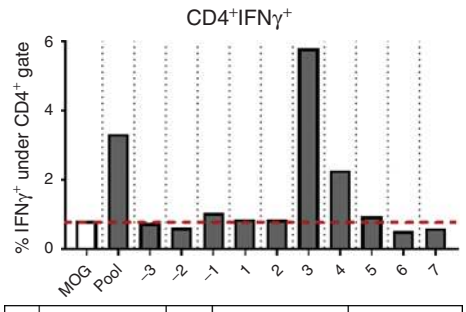

OLP	Allele	Rank	netmhciipan_IC50	sturniolo score
3	HLA-DRB1*04:02	2.79		2
3	HLA-DRB3*03:01	26.3	357.32	
4	HLA-DRB1*04:02	1.94		2.4

Donor 3, HLA typing		
	Class I	
A*	02:01:01	24:02:01
B*	49:01:01	49:01:01
C*	07:01:01	07:01:01
	Class II	
DRB1*	14:04:01	15:01:01
DRB3*	02:02:01	
DRB5*	01:01:01	
DQA1*	01:01:01	01:02:01
DQB1*	05:01:01	05:03:01
DPA1*	02:01:01	02:01:01
DPB1*	14:01:01	17:01:01

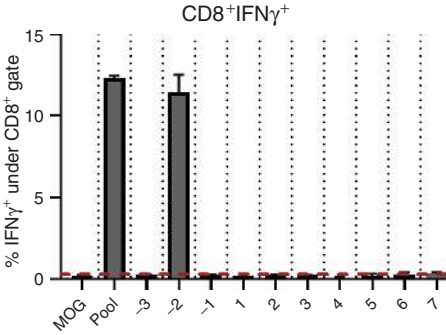

OLP	Allele	Epitope	Rank	ann_IC50	smm_IC50
–2	HLA-C*07:01	MRMRRMRRT	0.16	80.8	5.84
–2	HLA-C*07:01	MRTKMRMRR	1.36	2025.79	44.07
–2	HLA-C*07:01	MMRTKMRMR	9.9	6512.67	1.8

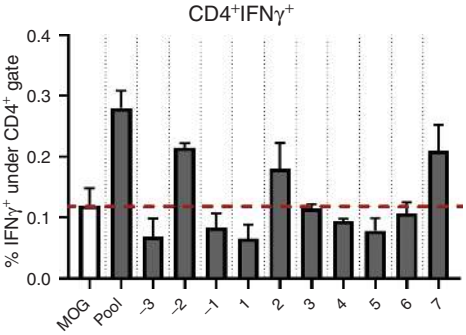

OLP	Allele	Rank	netmhciipan_ic50	nn_align_ic50
–2	HLA-DRB1*14:04	0.43	19.52	
–2	HLA-DRB5*01:01	2.98		33.5
2	HLA-DRB5*01:01	6.74		434.3

Figure 5. T cells recognize multiple epitopes in mut-CALR. PBMCs from 3 HDs, donors 1, 2, and 3, were stimulated *in vitro* with individual OLPs, and IFNγ production by CD8+ and CD4+ T cells was measured by flow cytometry. HLA alleles of individuals were identified by sequence-based genotyping. Binding affinities of donors' alleles to epitopes within the OLPs that induced IFNγ production were predicted by IEDB's recommended algorithm. ANN, artificial neural network (NetMHC 4.0); SMM, stabilized matrix method; NN-align, NetMHCII 2.2; SMM-align, NetMHCII 1.1.

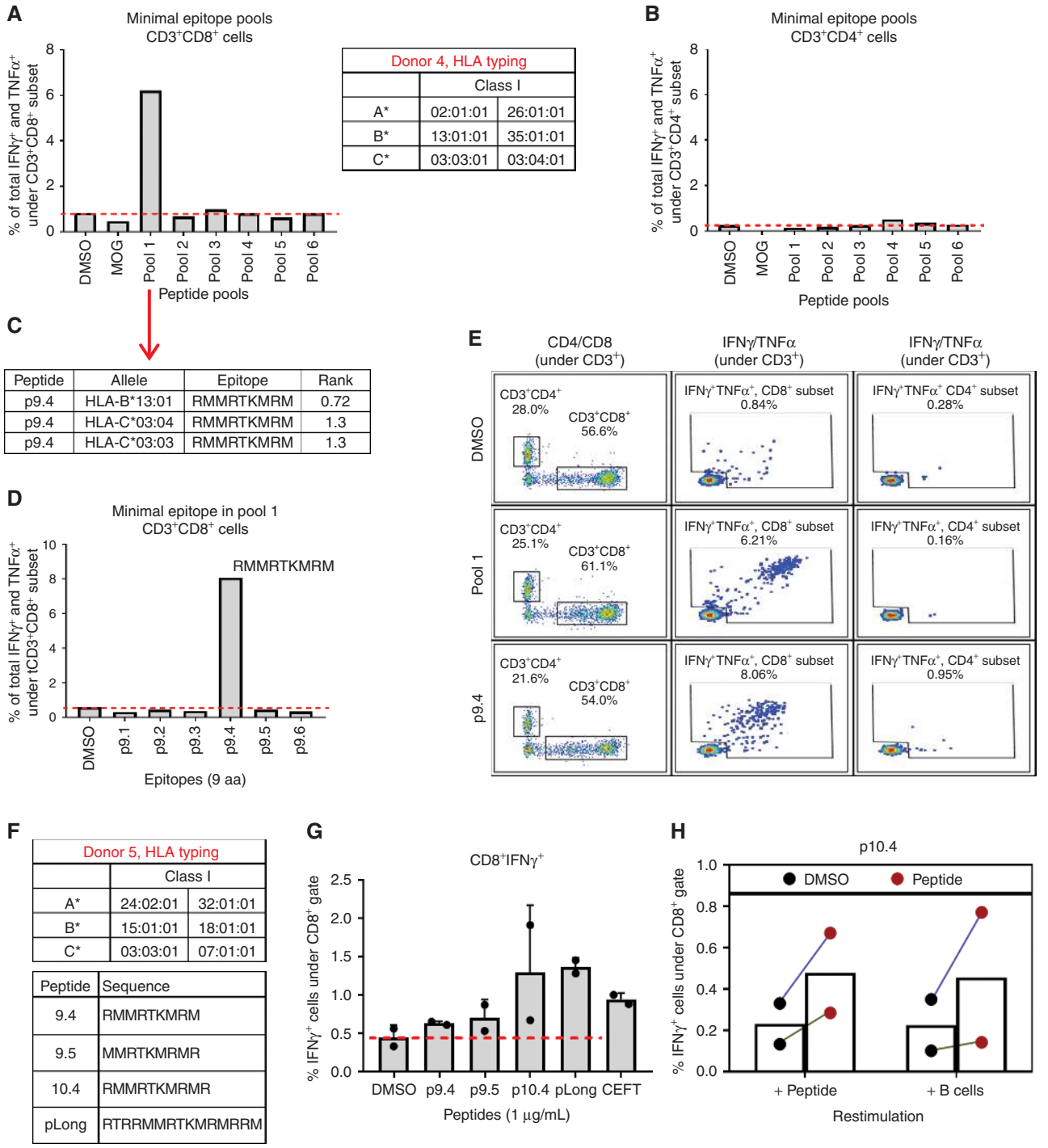

Donor 4, HLA typing		
	Class I	
A*	02:01:01	26:01:01
B*	13:01:01	35:01:01
C*	03:03:01	03:04:01

Peptide	Allele	Epitope	Rank
p9.4	HLA-B*13:01	RMMRTKMRM	0.72
p9.4	HLA-C*03:04	RMMRTKMRM	1.3
p9.4	HLA-C*03:03	RMMRTKMRM	1.3

Donor 5, HLA typing		
	Class I	
A*	24:02:01	32:01:01
B*	15:01:01	18:01:01
C*	03:03:01	07:01:01

Peptide	Sequence
9.4	RMMRTKMRM
9.5	MMRTKMRMR
10.4	RMMRTKMRMR
pLong	RTRRMMRTKMRMRRM

Figure 6. T cells recognize mut-CALR epitopes that are endogenously processed and presented. PBMCs from donor 4 were stimulated *in vitro* with pools of short peptides (9 aa and 6–7 peptides/pool) and frequencies of IFNγ and TNFα producing $CD8^+$ (**A**) and $CD4^+$ (**B**) T cells were measured by flow cytometry. HLA alleles of individuals were identified by sequence-based genotyping. **C,** Binding affinities of donor 4's alleles to the 6 epitopes within pool 1 were predicted by NetMHCPan 3.0. Epitopes with a predicted percentile rank <2 are listed. **D,** Donor 4 PBMCs were stimulated with individual short peptides constituting pool 1. Frequencies of IFNγ and TNFα producing $CD8^+$ T cells were measured by flow cytometry. **E,** Flow plots showing IFNγ and TNFα production by $CD8^+$ and $CD4^+$ T cells upon stimulation with p9.4. **F,** PBMCs from donor 5 were stimulated *in vitro* with peptides listed. **G,** Frequencies of IFNγ producing $CD8^+$ T cells were measured by flow cytometry. Data were pooled from two independent experiments. **H,** Donor 5 PBMCs expanded with p10.4 were restimulated either by the short peptide they were expanded with or by coculturing autologous B cells that were pulsed with pLong. DMSO or DMSO-pulsed B cells were used as background controls, respectively. Data were pooled from two independent experiments.

CALR mutations could be recognized *in vitro* by T cells from patients with *CALR*$^+$ MPN. However, the responses were restricted to CD4$^+$ T cells (36, 37). Tubb and colleagues focused on identifying mut-CALR epitopes recognized by CD8$^+$ T cells based on predicted epitope-MHC information. However, mut-CALR reactive CD8$^+$ T cells were elicited only in healthy donors but not in patients with MPN (38). In either case, the majority of predicted peptides failed to elicit T-cell responses and the observed mut-CALR–specific T-cell responses were weak. In the current study, we systematically evaluated the mut-CALR C-terminus for peptides binding to MHC molecules by using *in silico* MHC-I and MHC-II peptide binding prediction algorithms. We identified 103 peptides predicted to bind to representative MHC-I and MHC-II molecules with high affinity (Supplementary Tables S1 and S2). To account for MHC-restricted peptides that may have been missed or otherwise incorrectly assigned by *in silico* predictors (35), we utilized an unbiased screening approach based on overlapping peptides spanning the full length of the shared mut-CALR C-terminus. Screening was performed in parallel in patients with MPN and healthy donors to control for factors associated with disease burden that may inhibit mut-CALR–specific T cells. We demonstrated that several MHC-I and MHC-II restricted peptides from mut-CALR were recognized by CD8$^+$ and CD4$^+$ T cells.

Significantly, mut-CALR–specific T-cell responses were lower in magnitude and less prevalent in patients with MPN when compared with healthy donors. Several putative explanations for these observations were explored. We stratified the patients in our cohort according to their type of MPN and explored associations with the mut-CALR–specific T-cell responses. We observed that the majority of patients with mut-CALR–specific T-cell responses had ET. Although mut-CALR–specific T-cell responses were occasionally observed in patients with MF who had a prior history of ET, none of the patients with primary MF had detectable T-cell responses. ET can evolve to MF, which is associated with greater symptom burden, inferior prognosis, and higher number of somatic mutations (39). Consistent with Holmström and colleagues' report (37), these observations suggest that mut-CALR–specific T-cell responses may occur more frequently in patients with *CALR*$^+$ MPN with low symptom burden. In addition, some of the patients with MF in our cohort were being treated with ruxolitinib at the time their samples were used in this study. Ruxolitinib has been previously shown to inhibit T-cell responses (40). Therefore, it is possible that ruxolitinib treatment impaired the reactivity of mut-CALR–specific T cells in some patients in our cohort, a possibility being examined in separate experiments.

Systemic T-cell dysfunction is frequently observed in patients with cancer. The severity of T-cell exhaustion is associated with disease progression due to factors such as prolonged exposure to tumor antigens, which results in elevated expression of checkpoint receptors that directly inhibit T-cell function (41). On the basis of the observed association with disease burden, we hypothesized that systemic T-cell exhaustion may limit the ability to observe spontaneous mut-CALR–specific T-cell responses in some patients with *CALR*$^+$ MPN. In support of this hypothesis, we observed that T cells from patients with *CALR*$^+$ MPN exhibited elevated expression of immune checkpoint receptors PD-1 and CTLA4, which have been associated with T-cell exhaustion. Second, we found that, in patients with MPN, antibody-mediated blockade of PD-1 or CTLA4 signaling *ex vivo* rescued mut-CALR–specific T-cell responses. Third, we observed that mut-CALR reactive T cells can be produced from naïve T cells from healthy donors in greater frequencies, again suggesting a role for suppression of mut-CALR–specific T cells in patients with MPN. Finally, administration of pembrolizumab was shown to rescue mut-CALR–specific T-cell responses in a patient with *CALR*$^+$ MPN. Collectively, these data show that spontaneous mut-CALR–specific T-cell responses that occur in patients with *CALR*$^+$ MPN may be actively suppressed by immune checkpoint receptor signaling and that blockade of said inhibitors augments the mut-CALR–specific T-cell responses *in vitro* and *in vivo*.

However, mut-CALR–specific T-cell responses were restored upon blockade of PD-1 and CTLA4 signaling only in a subset of patients. Several mechanisms might underlie these observations. The patients in our MPN cohort were not selected based on their HLA type and exhibit diverse HLA alleles. Hence, the lack of mut-CALR–specific T-cell responses could be the absence of the HLA alleles binding to mut-CALR epitopes with high affinity. Also, checkpoint receptors other than PD-1 and CTLA4 might contribute to suppression of mut-CALR–specific T-cell responses. Phenotypic analysis showed that several checkpoint receptors, including LAG3 and TIM4, were also highly expressed in peripheral blood T cells of patients with *CALR*$^+$ MPN. Therefore, inhibition of such molecules could be beneficial in restoring mut-CALR–specific T-cell responses. Chronic antigen exposure can lead to terminal exhaustion with limited reinvigoration potential in later stages of disease (41); thus, earlier intervention would be a more favorable approach.

A key biomarker of response to PD-1 blockade is tumor mutational burden (TMB; refs. 3, 7). TMB for MPN has previously been reported to be significantly low, 1 to 32 mutations per patient (12). Hence, it can be argued that the activity of anti–PD-1 treatment in patients with MPN would be low. However, even tumors with low TMB have been shown to provide high-quality neoantigens that elicit antitumor T-cell responses (42). Recent work by Cristescu and colleagues corroborate such observations by demonstrating that factors, such as a T cell–inflamed microenvironment, can independently predict response to PD-1 blockade even when the TMB is low (43). We observed that pembrolizumab treatment led to an overall increase in the proportion of peripheral blood T cells and significant expansion of several T-cell clones. It is possible that some of the expanded clones target high-quality neoantigens, mut-CALR and potentially others. Although limited to one patient, these observations suggest that *in vivo* PD-1 blockade in patients with *CALR*$^+$ MPN may reinvigorate neoantigen-specific T cells.

Although we demonstrated that mut-CALR epitopes could be recognized by both CD8$^+$ and CD4$^+$ T cells from healthy donors, patient-derived mut-CALR–specific T cells were primarily CD4$^+$. We hypothesized that the lack of CD8$^+$ mut-CALR–specific T cells in patients with *CALR*$^+$ MPN was the result of inefficient antigen presentation by MHC class I. CALR is a chaperone protein critical for the folding and assembly of MHC class I molecules (20). CALR-deficient cells are reported to have reduced levels of cell-surface MHC class I expression as well as reduced efficiency in antigen presentation to cytotoxic T lymphocytes (19). Even a heterozygous expression of

the mut-CALR protein, as is the case with majority of patients with *CALR*$^+$ MPN, has been shown to lead to a significant, albeit small, reduction in surface expression of MHC class I molecules (44). However, we did not observe a reduction in the cell-surface expression of MHC class I molecules in either PBMCs or CD34$^+$ cells from patients with *CALR*$^+$ MPN as compared with HDs. Similarly, MHC class II expression was also intact in patients with *CALR*$^+$ MPN. Hence the paucity of anti–mut-CALR responses in patients with *CALR*$^+$ MPN cannot be explained by a reduction of MHC expression. Yet it remains possible that the presentation of mut-CALR on MHC class I may be compromised, which warrants further investigation to evaluate the impact of mut-CALR on peptide loading and presentation.

Among the current standard treatment options for patients with MPN, only hematopoietic stem cell transplantation (HSCT) is potentially curative (17). However, the application of HSCT is limited due to lack of appropriate donor options, the advanced age of patients, comorbidities, and poor functional status (45). Other treatment modalities, although they improve symptom burden, show only minimal effects in eliminating malignant clones and providing molecular remissions (21, 46, 47). Therefore, it is essential to identify new approaches that advance the treatment of patients with MPN. We anticipate that our findings will form the basis for three avenues of therapy. A neoantigen vaccine targeting the C-terminal of mut-CALR can be administered, perhaps as a prevention of progression strategy, given that the disease is long-standing in nature and affects longevity considerably later. Studies by several groups demonstrated that administration of neoantigen vaccines could induce neoantigen-specific T-cell priming and also boost spontaneous neoantigen-specific T-cell immunity in patients with melanoma (48–50). Alternatively, the vaccine may be given in combination with checkpoint inhibitors, as is being done in several clinical trials for solid tumors (NCT02897765). Finally, an adoptive T-cell therapy for the treatment of patients with MPN harboring mutated *CALR* may be feasible, in which the patients will receive autologous reinvigorated mut-CALR–specific T cells that are expanded *ex vivo*. Sequencing and cloning of patients' TCRs could also be used to transduce healthy donor HLA-matched T cells for an alternative form of adoptive cell therapy, an approach we are pursuing. These immunotherapy regimens could potentially establish an effective mut-CALR–specific T-cell immunity, which would target and eliminate *CALR*$^+$ malignant cells, thereby leading to improved clinical outcomes in this patient population. Because *CALR* mutations are the second most common MPN driver mutation and mut-CALR neopeptide is shared among patients carrying each type of *CALR* mutation (11), strategies targeting mut-CALR are anticipated to be applicable to a significant number of patients with MPN.

METHODS

Detailed materials and methods are provided in the Supplementary Material.

Patient Samples

The use of patient-derived specimens was approved by the Institutional Review Boards at Mount Sinai (HS#11-02054) and all patients provided written informed consent before the initiation of any study procedures. The specimens were provided by the Hematological Malignancies Tissue Bank (HMTB) of the Tisch Cancer Institute (New York, NY). Patient blood was collected by the clinical personnel and mononuclear cells (MNC) were isolated by HMTB personnel by Ficoll–Paque density gradient. All patients analyzed in this study were diagnosed with MPN and tested positive for a *CALR* or *JAK*^{V617F} mutation. Because of low viability of patient cells after thawing, only freshly isolated patient PBMCs were used in immunogenicity assays, unless noted otherwise. Therefore, assays were performed once for each patient. HD specimens were procured from the New York Blood Center as leukopak, and MNCs were isolated by density gradient centrifugation using Ficoll–Paque Plus (GE Healthcare). PBMCs were cryopreserved in human serum containing 10% DMSO. HD PBMCs were used after thawing and assays were repeated at least twice.

Neoepitope Predictions

Peptide predictions were performed using algorithms available at the immune epitope database (IEDB) and analysis resource (www.iedb.org). Unless indicated otherwise, the IEDB recommended method was selected to perform prediction analyses for both MHC-I and MHC-II binding. Epitopes that were assigned an IC_{50} value lower than 500 and/or percentile rank lower than 2 were considered high-affinity binders.

Peptide Synthesis

Custom peptide libraries for WT and mut-CALR peptides were chemically synthesized by JPT Peptide Technologies. Each peptide had >80% purity as determined by high-performance liquid chromatography. MOG and CEFT peptide pools were commercially available at JPT Peptide Technologies. Each peptide was resuspended in DMSO and used at a final concentration of 1 μg/mL.

Induction of Neoantigen Reactive T Cells

For the induction of antigen-specific T cells, a previously published method (18) was used with modifications. Briefly, unfractionated PBMCs were cultured in X-VIVO15 media (LONZA) with cytokines and were stimulated with peptide(s) (1 μg/mL) or equal volume of DMSO in the presence of adjuvants. Cells were expanded with IL2 (R&D Systems, 10 IU/mL) and IL7 (R&D Systems, 10 ng/mL) in RPMI media containing 10% human serum (Gibco; R10 media). Cells were fed every 2 to 3 days. After 9 to 11 days of culture, cells were harvested and all wells were pooled within group. After washing with R10 media, cells were restimulated with either MOG to account for background signal or with the test peptide(s) they were initially stimulated with (1 μg/mL) in the presence of anti-CD28 (1 μg/mL) and anti-CD49d (1 μg/mL) antibodies (BD Biosciences). As controls, some cells were stimulated with PMA (Sigma-Aldrich, 50 ng/mL) and ionomycin (Sigma-Aldrich, 1 μg/mL).

The same immunogenicity assay was utilized to induce antigen-specific T-cell responses when checkpoint receptors were inhibited with the following modifications: On day 2, when PBMCs were stimulated with peptides and adjuvants, anti–PD-1 (clone EH12.1) or anti-CTLA4 (clone BNI3) antibodies (no azide/low endotoxin mouse anti-human antibodies by BD Biosciences, both used at 10 μg/mL) or the same concentration of isotype controls, mouse IgG1, κ or IgG2a, κ, respectively, were also added.

Functional Analysis of T-cell Responses

For ELISPOT analysis, plates with mixed cellular ester membrane (Millipore) were coated with anti-IFNγ antibody (clone 1-D1k by Mabtech, used at 4 μg/mL) overnight at 4°C. Plates were washed 3 times with plain RPMI and blocked by incubating with R10 media at 37°C for at least 1 hour prior to addition of cells expanded in immunogenicity assay. Cells were seeded at either 5×10^4 or 10^5 per well in duplicates and restimulated as detailed above for 48 hours, and

plates were processed for IFNγ detection. Plates were first incubated with biotinylated anti-IFNγ antibody (clone 7-B6-1 by Mabtech, used at 0.2 μg/mL) for 2 hours at 37°C, then 1 hour at room temperature with streptavidin-AP conjugate (Roche, used at 0.75 U/mL) and lastly with the SigmaFast BCIP/NBT substrate for 10 minutes at room temperature. Plates were washed 6 times with PBS containing 0.05% Tween-20 and 3 times with water in between each step. Plates were scanned and analyzed by ImmunoSpot software.

For flow cytometry, cells expanded in the immunogenicity assay were seeded at 1–2 × 10^5 per well. One hour after restimulation, BD GolgiStop, containing monensin, and BD GolgiPlug, containing brefeldin A, were added to cells according to the manufacturer's suggestion. Twelve hours after the addition of protein transport inhibitors, cells were processed for flow cytometry. Cells were first stained for surface molecules with the following antibodies: anti-CD3 (OKT3), anti-CD4 (RPA-T4), anti-CD8 (RPA-T8), and anti-CD137 (4B4-1) and then processed for intracellular staining using BD Cytofix/Cytoperm reagents according to the manufacturer's protocol. Cells were then stained with anti-IFNγ (B27) and anti-TNFα (MAb11) antibodies. All antibodies were purchased from BioLegend.

TCR Sequencing

Longitudinal blood samples were available from a patient with *CALR*$^+$ MF (PT#15 in Supplementary Table S1) undergoing pembrolizumab treatment. PBMCs from this patient were isolated before and after 2 and 6 cycles of pembrolizumab treatment. PBMCs isolated after 2 cycles were expanded *in vitro* in an immunogenicity assay as described above by stimulating with WT or mut-CALR OLP pools, with or without PD-1 blocking mAbs. After expansion, cells were harvested. Genomic DNA was isolated from these 6 samples using DNeasy Blood and Tissue Kit (Qiagen) according to the manufacturer's instructions. The quality and quantity of the extracted DNA samples were analyzed by NanoDrop. DNA samples were sent to Adaptive Biotechnologies for TCR Vβ sequencing. Briefly, TCRβ CDR3 regions for each sample were amplified by a multiplexed PCR method using a mix of forward and reverse primers specific to TCR Vβ and TCR Jβ, respectively. Amplified regions were sequenced using the Illumina HiSeq System. Data analyses were performed using the Adaptive Biotechnologies ImmunoSeq Analyzer 3.0. Clonality was calculated as (1 − normalized entropy). Normalized entropy was defined as (Shannon entropy/$\log_2$R), where R = the total number of rearrangements. The frequency of T cells was calculated as (number of cells expressing TCR/number of total nucleated cells). Total nucleated cell numbers were obtained by converting the input DNA amount in the assay based on the assumption that each diploid cell has about 6.4 pg genomic DNA. In differential abundance analyses of TCRβ chain sequencing, only clones with a cumulative abundance of 10 or above were included. *P* values were calculated using the binomial method, and FDRs were controlled by the Benjamini–Hochberg method. *P* values ≤0.01 were considered statistically significant. The frequencies of VJ combinations for abundant clones were visualized using circular plots. To this end, the most abundant 50 clones at each time point were selected and the combination of these clones were mapped out. Circular plots were generated using circos software package (http://circos.ca/). Each arch represents a V or J allele. A joining ribbon indicates a unique VJ cassette combination. The arc length and the width of the ribbons indicate the frequency of V/J alleles and their cassette combination respectively.

Cell Lines

MARIMO cells were provided by N. Arshad and P. Cresswell (Yale School of Medicine, New Haven, CT). MARIMO cells were maintained at a density of 1–2 × 10^6 cells/mL in RPMI media (Gibco) containing 10% heat-inactivated FBS (Gibco) and penicillin–streptomycin (Gibco, used at 100 U/mL, 100 μg/mL, respectively). Cells were regularly tested for *Mycoplasma* contamination by PCR. The latest testing was performed in November 2018 and cells were negative for *Mycoplasma*.

Statistical Analyses

Statistical analyses performed were detailed in the figure legends. Briefly, statistical differences were assessed by Wilcoxon matched-pairs signed rank test or *t* test for comparisons between two groups. *P* values <0.05 were considered statistically significant. Statistical analyses were performed using GraphPad Prism software version 7 and 8. Differential abundance analyses of TCRβ chain sequencing data were performed using the Adaptive Biotechnologies ImmunoSeq Analyzer 3.0. *P* values were calculated using the binomial method and FDRs were controlled by the Benjamini–Hochberg method. *P* values ≤0.01 were considered statistically significant.

Disclosure of Potential Conflicts of Interest

J. Mascarenhas receives research support from Incyte, Novartis, CTI Biopharma, Janssen, and Roche, and is on the scientific advisory board for Celgene, Roche, and Incyte. R. Hoffman receives research support from Formation Biologics, Merus, Novartis, Roche/Genentech, Scholar Rock, and Elstar, and is on the scientific advisory board for Novartis. N. Bhardwaj reports receiving commercial research grants from Novocure, Celldex, Genentech, Oncovir, and Regeneron and other commercial research support from the Ludwig Institute, Cancer Research Institute, Leukemia & Lymphoma Society, and NYSTEM, and is a consultant/advisory board member for Neon, Tempest, Checkpoint Sciences, Curevac, PrimeVax, Array Biopharma, Roche, Avidea, and the Parker Institute for Cancer Immunotherapy. No potential conflicts of interest were disclosed by the other authors.

Authors' Contributions

Conception and design: C. Cimen Bozkus, J.P. Finnigan, R. Hoffman, C. Iancu-Rubin, N. Bhardwaj

Development of methodology: C. Cimen Bozkus, J.P. Finnigan, R. Hoffman, C. Iancu-Rubin, N. Bhardwaj

Acquisition of data (provided animals, acquired and managed patients, provided facilities, etc.): C. Cimen Bozkus, J. Mascarenhas, R. Hoffman, C. Iancu-Rubin, N. Bhardwaj

Analysis and interpretation of data (e.g., statistical analysis, biostatistics, computational analysis): C. Cimen Bozkus, V. Roudko, C. Iancu-Rubin, N. Bhardwaj

Writing, review, and/or revision of the manuscript: C. Cimen Bozkus, V. Roudko, J.P. Finnigan, J. Mascarenhas, R. Hoffman, C. Iancu-Rubin, N. Bhardwaj

Administrative, technical, or material support (i.e., reporting or organizing data, constructing databases): C. Cimen Bozkus, R. Hoffman, C. Iancu-Rubin

Study supervision: C. Iancu-Rubin, N. Bhardwaj

Acknowledgments

We thank N. Arshad and P. Cresswell (Yale School of Medicine) for providing the MARIMO cells and C. McClain (Tisch Cancer Institute at the Icahn School of Medicine at Mount Sinai) for performing *Mycoplasma* testing of the MARIMO cells. We also thank J. Arandela at HMTB (Tisch Cancer Institute at the Icahn School of Medicine at Mount Sinai) for assistance in specimen processing. Research funds were provided by the Myeloproliferative Neoplasms Research Foundation and Leukemia & Lymphoma Society to C. Iancu-Rubin and N. Bhardwaj and by the Parker Institute for Cancer Immunotherapy to N. Bhardwaj. Human specimens were provided by the HMTB of the Tisch Cancer Institute supported by the NCI P30 Cancer Center Support Grant P30 CA196521.

The costs of publication of this article were defrayed in part by the payment of page charges. This article must therefore be hereby

marked *advertisement* in accordance with 18 U.S.C. Section 1734 solely to indicate this fact.

Received November 21, 2018; revised May 8, 2019; accepted June 27, 2019; published first July 2, 2019.

REFERENCES

1. Rosenberg SA, Restifo NP. Adoptive cell transfer as personalized immunotherapy for human cancer. Science 2015;348:62–8.
2. Sharma P, Allison JP. The future of immune checkpoint therapy. Science 2015;348:56–61.
3. Hellmann MD, Ciuleanu TE, Pluzanski A, Lee JS, Otterson GA, Audigier-Valette C, et al. Nivolumab plus Ipilimumab in Lung Cancer with a High Tumor Mutational Burden. N Engl J Med 2018;378:2093–104.
4. Larkin J, Chiarion-Sileni V, Gonzalez R, Grob JJ, Cowey CL, Lao CD, et al. Combined nivolumab and ipilimumab or monotherapy in untreated melanoma. N Engl J Med 2015;373:23–34.
5. Engels B, Engelhard VH, Sidney J, Sette A, Binder DC, Liu RB, et al. Relapse or eradication of cancer is predicted by peptide-major histocompatibility complex affinity. Cancer Cell 2013;23:516–26.
6. Rizvi NA, Hellmann MD, Snyder A, Kvistborg P, Makarov V, Havel JJ, et al. Cancer immunology. Mutational landscape determines sensitivity to PD-1 blockade in non-small cell lung cancer. Science 2015;348:124–8.
7. Yarchoan M, Hopkins A, Jaffee EM. Tumor mutational burden and response rate to PD-1 inhibition. N Engl J Med 2017;377:2500–1.
8. Le DT, Durham JN, Smith KN, Wang H, Bartlett BR, Aulakh LK, et al. Mismatch repair deficiency predicts response of solid tumors to PD-1 blockade. Science 2017;357:409–13.
9. Capietto AH, Jhunjhunwala S, Delamarre L. Characterizing neoantigens for personalized cancer immunotherapy. Curr Opin Immunol 2017;46:58–65.
10. Schumacher TN, Schreiber RD. Neoantigens in cancer immunotherapy. Science 2015;348:69–74.
11. Klampfl T, Gisslinger H, Harutyunyan AS, Nivarthi H, Rumi E, Milosevic JD, et al. Somatic mutations of calreticulin in myeloproliferative neoplasms. N Engl J Med 2013;369:2379–90.
12. Nangalia J, Massie CE, Baxter EJ, Nice FL, Gundem G, Wedge DC, et al. Somatic CALR mutations in myeloproliferative neoplasms with nonmutated JAK2. N Engl J Med 2013;369:2391–405.
13. Elf S, Abdelfattah NS, Baral AJ, Beeson D, Rivera JF, Ko A, et al. Defining the requirements for the pathogenic interaction between mutant calreticulin and MPL in MPN. Blood 2018;131:782–6.
14. Elf S, Abdelfattah NS, Chen E, Perales-Paton J, Rosen EA, Ko A, et al. Mutant calreticulin requires both its mutant c-terminus and the thrombopoietin receptor for oncogenic transformation. Cancer Discov 2016;6:368–81.
15. Luo W, Yu Z. Calreticulin (CALR) mutation in myeloproliferative neoplasms (MPNs). Stem Cell Investig 2015;2:16.
16. Ha JS, Kim YK. Calreticulin exon 9 mutations in myeloproliferative neoplasms. Ann Lab Med 2015;35:22–7.
17. Deeg HJ, Bredeson C, Farnia S, Ballen K, Gupta V, Mesa RA, et al. Hematopoietic cell transplantation as curative therapy for patients with myelofibrosis: long-term success in all age groups. Biol Blood Marrow Transplant 2015;21:1883–7.
18. Lissina A, Briceno O, Afonso G, Larsen M, Gostick E, Price DA, et al. Priming of qualitatively superior human effector CD8+ T cells using TLR8 ligand combined with FLT3 ligand. J Immunol 2016;196:256–63.
19. Gao B, Adhikari R, Howarth M, Nakamura K, Gold MC, Hill AB, et al. Assembly and antigen-presenting function of MHC class I molecules in cells lacking the ER chaperone calreticulin. Immunity 2002;16:99–109.
20. Raghavan M, Wijeyesakere SJ, Peters LR, Del Cid N. Calreticulin in the immune system: ins and outs. Trends Immunol 2013;34:13–21.
21. Koschmieder S, Mughal TI, Hasselbalch HC, Barosi G, Valent P, Kiladjian JJ, et al. Myeloproliferative neoplasms and inflammation: whether to target the malignant clone or the inflammatory process or both. Leukemia 2016;30:1018–24.
22. Bellucci S, Harousseau JL, Brice P, Tobelem G. Treatment of essential thrombocythaemia by alpha 2a interferon. Lancet 1988;2:960–1.
23. Silver RT, Vandris K, Goldman JJ. Recombinant interferon-alpha may retard progression of early primary myelofibrosis: a preliminary report. Blood 2011;117:6669–72.
24. Kollmann K, Nangalia J, Warsch W, Quentmeier H, Bench A, Boyd E, et al. MARIMO cells harbor a CALR mutation but are not dependent on JAK2/STAT5 signaling. Leukemia 2015;29:494–7.
25. Vannucchi AM, Rotunno G, Bartalucci N, Raugei G, Carrai V, Balliu M, et al. Calreticulin mutation-specific immunostaining in myeloproliferative neoplasms: pathogenetic insight and diagnostic value. Leukemia 2014;28:1811–8.
26. Zarour HM. Reversing T-cell Dysfunction and Exhaustion in Cancer. Clin Cancer Res 2016;22:1856–64.
27. Wang JC, Kundra A, Andrei M, Baptiste S, Chen C, Wong C, et al. Myeloid-derived suppressor cells in patients with myeloproliferative neoplasm. Leuk Res 2016;43:39–43.
28. Huang AC, Postow MA, Orlowski RJ, Mick R, Bengsch B, Manne S, et al. T-cell invigoration to tumour burden ratio associated with anti-PD-1 response. Nature 2017;545:60–5.
29. Kamphorst AO, Pillai RN, Yang S, Nasti TH, Akondy RS, Wieland A, et al. Proliferation of PD-1+ CD8 T cells in peripheral blood after PD-1-targeted therapy in lung cancer patients. Proc Natl Acad Sci U S A 2017;114:4993–8.
30. Simoni Y, Becht E, Fehlings M, Loh CY, Koo SL, Teng KWW, et al. Bystander CD8(+) T cells are abundant and phenotypically distinct in human tumour infiltrates. Nature 2018;557:575–9.
31. Stronen E, Toebes M, Kelderman S, van Buuren MM, Yang W, van Rooij N, et al. Targeting of cancer neoantigens with donor-derived T cell receptor repertoires. Science 2016;352:1337–41.
32. Beck R, Lam-Po-Tang PR. Comparison of cord blood and adult blood lymphocyte normal ranges: a possible explanation for decreased severity of graft versus host disease after cord blood transplantation. Immunol Cell Biol 1994;72:440–4.
33. Gonzalez-Galarza FF, Takeshita LY, Santos EJ, Kempson F, Maia MH, da Silva AL, et al. Allele frequency net 2015 update: new features for HLA epitopes, KIR and disease and HLA adverse drug reaction associations. Nucleic Acids Res 2015;43:D784–8.
34. Gragert L, Madbouly A, Freeman J, Maiers M. Six-locus high resolution HLA haplotype frequencies derived from mixed-resolution DNA typing for the entire US donor registry. Hum Immunol 2013;74:1313–20.
35. The problem with neoantigen prediction. Nat Biotechnol 2017;35:97.
36. Holmstrom MO, Martinenaite E, Ahmad SM, Met O, Friese C, Kjaer L, et al. The calreticulin (CALR) exon 9 mutations are promising targets for cancer immune therapy. Leukemia 2018;32:429–37.
37. Holmstrom MO, Riley CH, Svane IM, Hasselbalch HC, Andersen MH. The CALR exon 9 mutations are shared neoantigens in patients with CALR mutant chronic myeloproliferative neoplasms. Leukemia 2016;30:2413–6.
38. Tubb VM, Schrikkema DS, Croft NP, Purcell AW, Linnemann C, Freriks MR, et al. Isolation of T cell receptors targeting recurrent neoantigens in hematological malignancies. J Immunother Cancer 2018;6:70.
39. Rumi E, Cazzola M. Diagnosis, risk stratification, and response evaluation in classical myeloproliferative neoplasms. Blood 2017;129:680–92.
40. Parampalli Yajnanarayana S, Stubig T, Cornez I, Alchalby H, Schonberg K, Rudolph J, et al. JAK1/2 inhibition impairs T cell function in vitro and in patients with myeloproliferative neoplasms. Br J Haematol 2015;169:824–33.
41. Wherry EJ. T cell exhaustion. Nat Immunol 2011;12:492–9.
42. Balachandran VP, Luksza M, Zhao JN, Makarov V, Moral JA, Remark R, et al. Identification of unique neoantigen qualities in long-term survivors of pancreatic cancer. Nature 2017;551:512–6.
43. Cristescu R, Mogg R, Ayers M, Albright A, Murphy E, Yearley J, et al. Pan-tumor genomic biomarkers for PD-1 checkpoint blockade-based immunotherapy. Science 2018;362.
44. Arshad N, Cresswell P. Tumor-associated calreticulin variants functionally compromise the peptide loading complex and impair its recruitment of MHC-I. J Biol Chem 2018;293:9555–69.

45. Kroger NM, Deeg JH, Olavarria E, Niederwieser D, Bacigalupo A, Barbui T, et al. Indication and management of allogeneic stem cell transplantation in primary myelofibrosis: a consensus process by an EBMT/ELN international working group. Leukemia 2015;29:2126–33.
46. Devlin R, Gupta V. Myelofibrosis: to transplant or not to transplant? Hematol Am Soc Hematol Educ Program 2016;2016:543–51.
47. Harrison C, Kiladjian JJ, Al-Ali HK, Gisslinger H, Waltzman R, Stalbovskaya V, et al. JAK inhibition with ruxolitinib versus best available therapy for myelofibrosis. N Engl J Med 2012;366:787–98.
48. Carreno BM, Magrini V, Becker-Hapak M, Kaabinejadian S, Hundal J, Petti AA, et al. Cancer immunotherapy. A dendritic cell vaccine increases the breadth and diversity of melanoma neoantigen-specific T cells. Science 2015;348:803–8.
49. Ott PA, Hu Z, Keskin DB, Shukla SA, Sun J, Bozym DJ, et al. An immunogenic personal neoantigen vaccine for patients with melanoma. Nature 2017;547:217–21.
50. Sahin U, Derhovanessian E, Miller M, Kloke BP, Simon P, Lower M, et al. Personalized RNA mutanome vaccines mobilize poly-specific therapeutic immunity against cancer. Nature 2017;547:222–6.